Available online at www.sciencedirect.com
SCIENCE DIRECT®
Surface Science 565 (2004) 151–162
SURFACE SCIENCE
www.elsevier.com/locate/susc

Examination of the oxidation of iron by oxygen using X-ray photoelectron spectroscopy and QUASES™

A.P. Grosvenor [a,b,*], B.A. Kobe [a], N.S. McIntyre [a,b]

[a] *Surface Science Western, Room G-1, Western Science Centre, The University of Western Ontario, London, Ont., Canada N6A 5B7*
[b] *Department of Chemistry, The University of Western Ontario, London, Ont., Canada N6A5B7*

Received 22 March 2004; accepted for publication 21 June 2004
Available online 21 July 2004

Abstract

Oxidation of iron (Fe) by oxygen (O_2) at low pressures was investigated using XP spectra and QUASES™ Analyze and Generate software programs. The results indicated that the oxide films produced after short oxygen exposure times contained a mixture of magnetite (Fe_3O_4) and maghemite (γ-Fe_2O_3) without distinct interfaces between the two being seen. Further investigation suggested that a reaction mechanism involving cationic diffusion was mostly responsible for the formation of Fe_3O_4, while a mechanism involving anionic diffusion was responsible for γ-Fe_2O_3 growth. The kinetics of the overall reaction were also investigated and found to follow a direct logarithmic relationship with increasing time. The rates of oxide growth were calculated for different pressures studied at the same temperature and found to be the same. This observation was used to conclude that the rate-limiting step was the formation of a thin oxide film by place-exchange and not anionic or cationic diffusion.
© 2004 Elsevier B.V. All rights reserved.

Keywords: X-ray photoelectron spectroscopy; Iron; Oxidation; Tunneling

1. Introduction

The near surface structures produced during oxidation of iron have received great attention in the past [1–9]. Exposure of iron to low pressures of dry oxygen gas at room temperature results in an oxide that has been reported to consist qualitatively of a layer of Fe_3O_4 covered by a second layer of γ-Fe_2O_3 [4–6]. Other researchers examining the oxidation of single crystal Fe(1 0 0) have suggested that a mixture of oxides rather than distinct oxide layers are found [7]. Kinetic studies performed by Graham et al. [9] using a manometric method to measure oxygen uptake at temperatures between

* Corresponding author. Surface Science Western, Room G-1, Western Science Centre, The University of Western Ontario, London, Ont., Canada N6A 5B7. Tel.: +1 519 661 2173/2111; fax: +1 519 661 3709.
E-mail address: agrosven@uwo.ca (A.P. Grosvenor).

0039-6028/$ - see front matter © 2004 Elsevier B.V. All rights reserved.
doi:10.1016/j.susc.2004.06.210

25 and 300 °C found that the oxide formation followed a logarithmic function with increasing time. The oxide in this study was assumed to be uniquely Fe_3O_4 and the amount of oxide formed was found to increase as the surfaces were changed from single crystal to polycrystalline [9]. These kinetic results have been confirmed at temperatures below 200 °C using XPS [10]. Above 200 °C, however, plots of oxide thickness versus oxygen exposure have shown a greatly increased slope indicating a probable change in mechanism [10]. Oxidation studies of Fe carried out in O_2 at pressures of less than 1×10^5 Pa and temperatures ranging from 800 to 1000 °C have indicated that the oxidation kinetics obeyed a parabolic law [11].

X-ray photoelectron spectroscopy (XPS) has been used heavily to determine surface oxide composition and to measure changes in oxide thickness [10,12–14]. In the past, XPS has had limited capacity to probe compositions and structures beneath the outermost oxide and to provide a well defined measure of the interfaces that are known or expected to be present following a reaction of metal and oxygen. However, the development of methods to analyze the extrinsic loss structure present in all XP spectra [15,16] appears poised to increase the density of information available on surface structures. Specifically, such methods seem capable of providing much improved definition, both to the identification of oxide structures as well as their thicknesses.

Research in this laboratory using XPS and QUASES™ Generate and Analyze [17] software programs has shown that the QUASES™ algorithms are suitable for studying the oxidation of Fe [18]. These algorithms are used to model the extrinsic loss structures found in XP spectra, and from this, determine the depth at which the loss signals originate [15]. "Analyze" models the extrinsic background of a photoelectron peak, allowing one to determine the range of depth at which the bulk structure originated. "Generate", on the other hand, allows the experimental spectra to be modelled using various combinations of reference spectra whose extrinsic backgrounds have been altered based on the depth at which they are found within the surface [17,18]. The accuracy of the thickness determined is dependent upon the attenuation length and the energy loss function (inelastic electron scattering cross-section) used. The initial oxidation study of Fe using several pressures of O_2 [18] showed that the oxide layer did, in fact, contain a layered mixture of the oxides Fe_3O_4 and γ-Fe_2O_3.

This paper reports a comprehensive study of the effect of time, temperature and pressure on the growth of surface oxides during exposure of polycrystalline Fe to O_2. The initiation of metal oxidation at low temperature has been suggested to result from field induced electron transport/tunnelling under constant potential from the metal through an existing thin oxide film to adsorbed oxygen [8]. The oxide initially grows quickly, with the rate flattening out when the potential across the layer starts to become significantly low [2]. From this model, an inverse logarithmic growth versus time relationship has been derived:

$$\frac{dx}{dt} = N\Omega v e^{-\frac{(W-qaE)}{kT}} \quad (1)$$

where x = oxide thickness, t = time, N = potential number of mobile ions, Ω = oxide volume per mobile ion, v = atomic vibration frequency, W = energy barrier to ion movement into the oxide, q = ionic charge (Ze), a = half the ion jump distance, E = the electric field (V/x), k = Boltzmann's constant, and T = the temperature at which the reaction occurs [2]. The integrated equation is usually represented as $\frac{1}{x} = -\left|\frac{kT}{qaV}\right| \ln t + \text{constant}$ [2].

Direct logarithmic kinetics proposed by Eley and Wilkinson [19] also allows for an electron tunnelling mechanism, but for film growth under constant field conditions:

$$\frac{dx}{dt} = aP^{0.6}e^{-bx} = Ae^{-\frac{E}{RT}}P^{0.6}e^{-\frac{\gamma x}{RT}} \quad (2)$$

where A = the pre-exponential value, E = activation energy, P = reaction pressure, T = temperature, x = thickness of the oxide at time t, and γ = increase in activation free energy with thickness of the oxide film [19]. The inclusion of P in the equation indicates the importance of the oxygen concentration to the reaction and is thus more appropriate for a mechanism involving anion diffusion [2].

This paper describes the oxidation of Fe under low temperature ($\leqslant 150$ °C) and pressure conditions. Specific attention will be paid to the individual reactions governing the growth of Fe_3O_4 and γ-Fe_2O_3. The kinetics of the reaction will be shown to be modelled best using a logarithmic equation.

2. Experimental

2.1. Sample preparation

Pure polycrystalline iron rod (99.995%) from Alfa-Aesar was cut into 3.4 mm disks using a diamond saw with one surface being polished to a mirror finish using 0.05 μm γ-Al_2O_3. Samples were degreased in methanol using an ultrasonic cleaner and then loaded into a Kratos AXIS Ultra XPS for oxygen treatment and analysis. All samples were cleaned again in the vacuum chamber of the Kratos spectrometer first by sputter cleaning the surface for 10 min using a 4 kV Ar^+ ion beam, then by annealing in vacuum at 600 °C for 30 min. After in vacuo cleaning, all samples were analyzed by XPS to confirm that all contaminate species (C, Na, etc.) had been removed and that no oxides remained.

After the surface was determined to be free of oxides, it was transferred into another vacuum chamber of the XPS where the dosing experiments were performed. Before the sample was placed in this chamber, a residual gas analyzer was first used to determine the gas partial pressures in the chamber. Although water vapour had the highest partial pressure (typically 10^{-6} Pa) of the residual gases, this was 10^4 times lower than the O_2 pressures used during reaction ($>10^{-2}$ Pa). To rule out that any of the reaction products found during this study were from the reaction of Fe and water vapour, a clean Fe disk was exposed to the residual gases found in the reaction chamber for 2 min and than analyzed by XPS. No oxide or hydroxide species were found indicating that the background contamination present in the reaction chamber was not concentrated enough to react with the Fe. This result follows those shown in a previous study which indicated that water vapour is much less reactive towards Fe than oxygen gas is after equivalent exposures [20]. The vacuum in the reaction chamber was controlled using multiple turbo-molecular pumps.

2.2. Reactions

To oxidize the clean Fe surface, medical grade oxygen (Praxair) dried by passage through a silica gel column (6–8 mesh, EM Science) was used. The polyvinyl tube used to carry the oxygen into the instrument from the gas cylinder was pumped out under vacuum for 24 h prior to beginning the study to remove as much adsorbate contamination as possible. After introduction into the vacuum chamber where dosing was performed, the samples were exposed to the reactant gas for 120 s at pressures of 1.3×10^{-2}, 1.3, and 1.3×10^2 Pa measured using a Pirani gauge and temperatures of 27 ± 2 and 150 ± 1 °C. The total dose in Langmuirs (L) was calculated by using the average pressure of O_2 that the surface experienced. The reaction kinetics were also observed at oxygen dosing pressures of 1.3×10^{-2} and 1.3 Pa. The exposure times were 20, 200, and 2000 s with the temperature held at 27 ± 1 °C. When oxidizing the samples, a certain amount of time was always required to increase the O_2 pressure to the wanted value. Although the amount of O_2 to which the surface was exposed was very small, it cannot be ruled out that some oxide did in fact form during this time period. After dosing, the samples were returned to the analytical chamber and analyzed using the following conditions; monochromatic Al Kα X-ray source, binding energy (BE) range = 1100–0 eV, step size = 0.7 eV, pass $E = 160$ eV, sweep time = 180 s, and number of sweeps = 8. High resolution spectra were also taken for Fe 2p, O 1s, and C 1s using a 20–40 eV window, depending on the peak analyzed, and a pass energy of 40 eV. The transfer lens was used in electrostatic mode due to the ferromagnetic properties of Fe.

2.3. Data analysis

All spectra were first analyzed using the CasaXPS software [21]. After being oxidized, all of the surfaces analyzed were found to contain small concentrations of adventitious C on the surface.

Peak shifts due to any apparent charging were normalized with the C 1s peak set to 284.8 eV. The Fe 2p high resolution spectra were fitted using Gupta–Sen multiplet peaks [22–25]. The Fe^{3+}/Fe^{2+} peak ratio was allowed to vary since Fe_2O_3 is known to form, as well as Fe_3O_4, in these conditions [3,18]. Any Fe metal component found (BE = 707 eV) was fitted using a Doniach and Sunjic asymmetric synthetic peak corresponding to interactions of conduction electrons with the core hole [26]. The peak full width at half maximum (FWHM) was generally held to be between 1.0 and 1.2 eV. The width used was determined by matching the low BE slope of the synthetic peak to that of the spectrum. The O 1s high resolution spectra were also examined for the presence of O^{2-} near 530 eV [4,27] and other oxygen species at binding energies extending from 531 to 532 eV.

2.4. QUASES^{TM}

To determine the approximate oxide layer depth, QUASES^{TM} Analyze was used to assess the oxide thickness from the O 1s extrinsic loss structure. The attenuation lengths used in the QUASES^{TM} computations were approximated by inelastic mean free path (IMFP, λ) values determined using the TPP-2M equation [28]. The value for O 1s was determined using Fe_3O_4 as the model compound and a kinetic energy of 956 eV. The IMFP (λ_{O1s}) determined was 1.93 nm. The universal cross-section developed by Tougaard [29] was used for all species analyzed.

Generate was used to determine the depth of individual oxide layers using the Fe 2p region on the basis of the appropriate reference spectra obtained previously. Reference samples used were the same as those discussed in Ref. [18]. Spectra from the reference compounds were all used either separately or in combination to model the experimental spectra under consideration. The surfaces were always modelled in such a way that the $Fe^{(0)}$ metal spectra remained as the bulk, overlaid by Fe^{2+} compounds, followed by the Fe^{3+} compounds that were closest to the surface. A spectrum was deemed to have been adequately fitted if the model spectra almost or completely overlaid the extrinsic background region of the experimental spectra located between kinetic energies of 720 and 750 eV. Further information on the methodology used when fitting the spectra using either Generate or Analyze can be found in Ref. [18].

The IMFP values used for the Fe 2p photoelectrons from the metal and oxides were: $\lambda_{Fe} = 1.57$ nm, $\lambda_{Fe_3O4} = 1.65$ nm, and $\lambda_{Fe_2O3} = 1.65$ nm. During our initial investigations [18], an experimental attenuation length was determined for the Fe 2p photoelectron of the γ-Fe_2O_3/Fe_3O_4 oxide. This was done by an independent measurement of this oxide thickness using nuclear reaction analysis (NRA). The value of the attenuation length determined from the NRA experiment (1.38 nm) was found to be approximately 20% lower than the IMFP value calculated using the TPP-2M equation (1.65 nm) [18]. All thicknesses listed below were altered to reflect this difference.

3. Results

3.1. Effects of O_2 dose over a range of pressures: 27 and 150 °C

Fig. 1 shows the Fe $2p_{3/2}$ photoelectron spectrum following oxidation at pressures of 0, 1.3×10^{-2}, 1.3, and 1.3×10^{2} Pa O_2 at 27 °C. The oxide portion of the spectra was consistently observed to contain the oxide species Fe_3O_4 and Fe_2O_3, with no detectable presence of FeO. Fig. 2 shows the equivalent Fe $2p_{3/2}$ spectra for these pressures at an oxidation temperature of 150 °C; the effect of the higher temperature is clearly evident.

For all oxygen exposures, the extrinsic background associated with the O 1s line was first analyzed to determine the distribution of the oxygen density as a function of depth. This was done using the QUASES^{TM} Analyze software program and a λ value of 1.93 nm for the O 1s electrons. Fig. 3 shows a typical analysis of the extrinsic background including the separation of the intrinsic portion of the spectrum.

From this O 1s study, a total thickness of oxygen through the surface structure was determined. This would include oxygen formed as a solid oxide as well as interstitial oxygen within the metal and

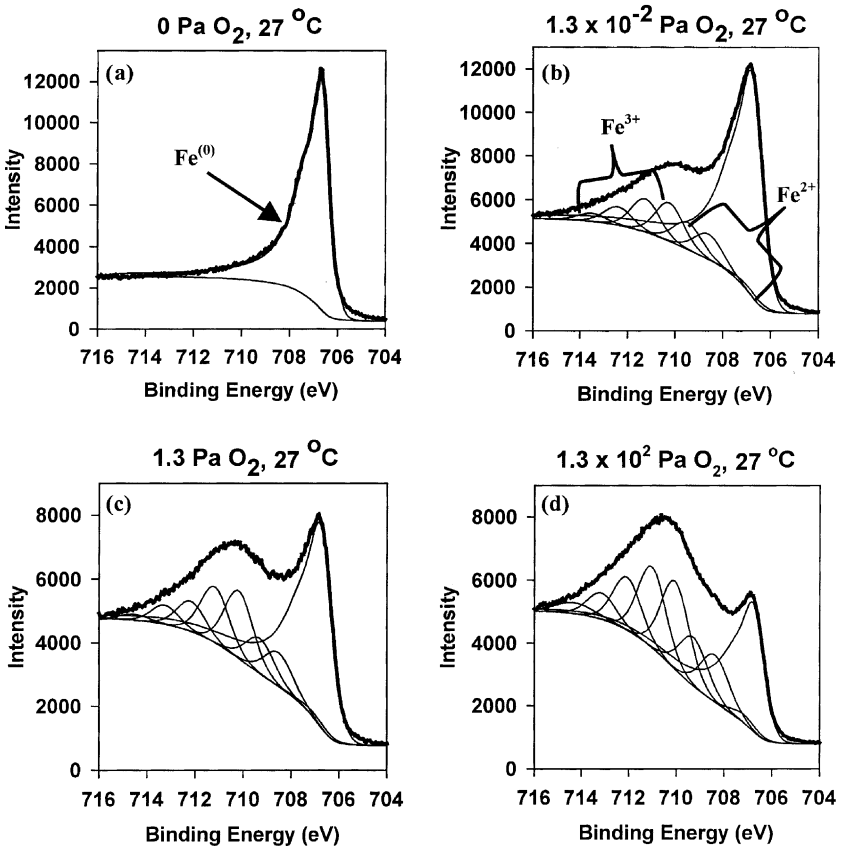

Fig. 1. Fe $2p_{3/2}$ photoelectron spectra following exposure to oxygen pressures of: (a) 0 Pa O_2, (b) 1.3×10^{-2} Pa O_2, (c) 1.3 Pa O_2, (d) 1.3×10^2 Pa O_2 at a temperature of 27 ± 2 °C.

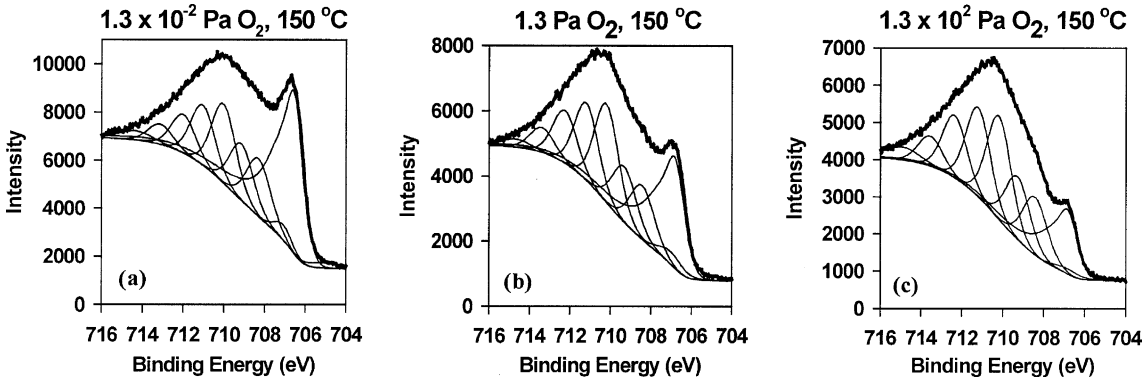

Fig. 2. Fe $2p_{3/2}$ photoelectron spectra following exposures to oxygen pressures of: (a) 1.3×10^{-2} Pa O_2, (b) 1.3 Pa O_2, (c) 1.3×10^2 Pa O_2 at a temperature of 150 ± 1 °C.

adsorbate oxygen at or near the metal surface. The results of calculated oxygen thicknesses are shown in Fig. 4 for triplicate O_2 doses of Fe at three distinct pressures and two different temperatures. A

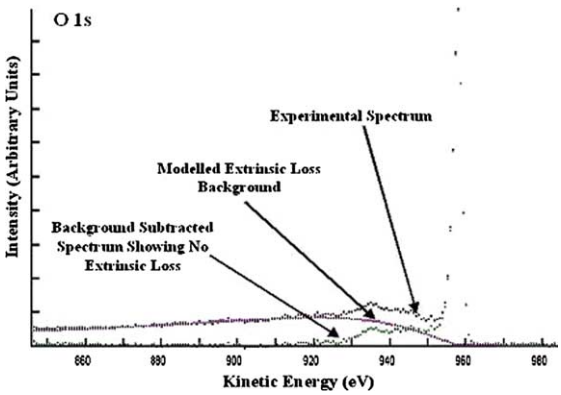

Fig. 3. Representative QUASES^{TM} Analyze analysis of an O 1s spectrum from an Fe surface after exposure to 1.3×10^2 Pa O_2 for 120 s at a temperature of 27 ± 2 °C. An oxide thickness of 3.3 nm was determined to be present.

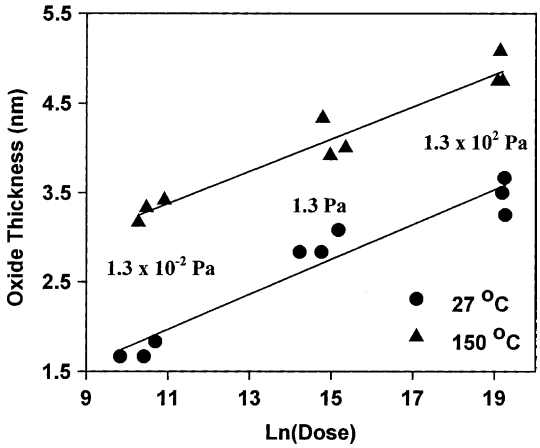

Fig. 4. Change in the overall oxide thickness for oxygen doses of 1.3×10^{-2}–1.3×10^2 Pa as determined using QUASES^{TM} Analyze. The results were found to follow a direct logarithmic relationship. The average goodness of fit for the direct logarithmic plot found using an R^2 value was 0.94 where as it was found to be 0.91 and 0.70, respectively, for inverse logarithmic and parabolic plots.

direct logarithmic relationship between the oxide thickness and dose was found to be the best fit for both temperatures studied. The slope of the growth curve was found to be very similar at each temperature. The oxidation trends found here are very similar to those observed by Graham et al. [9] and Srinivasan et al. [10].

QUASES^{TM} Generate was used to determine the composition and thickness of individual oxides formed during oxidation. Three different iron phases were used to model the experimental extrinsic background (Fe metal, Fe_3O_4, γ-Fe_2O_3) of a Fe 2p spectrum from an iron surface after oxidation, as is shown in Fig. 5. The Generate program allows the thicknesses of each of these phases to be varied in such a way as to achieve a close fit to the experimental spectra. Contributions from other possible oxide phases, such as α-Fe_2O_3, were also explored; no significant contribution was found [18]. The Fe 2p peak and its loss structure found in the modelled spectra correlates well with the experimental spectra in the region of 720–790 eV, which was the main area of interest; some fitting difficulty in the region between 700 and 720 eV was ascribed to the Fe LMM Auger contribution found in this range.

Some of the modelled oxide phase distributions obtained are shown in Fig. 6 for O_2 exposures of Fe at both 27 and 150 °C. For each case, the vertical axis represents depth. The oxide phase located adjacent to the metal/oxide interface was found to be Fe_3O_4. γ-Fe_2O_3 was identified as a separate phase on the outermost surface of most of the oxidized samples. A region of mixed Fe_3O_4

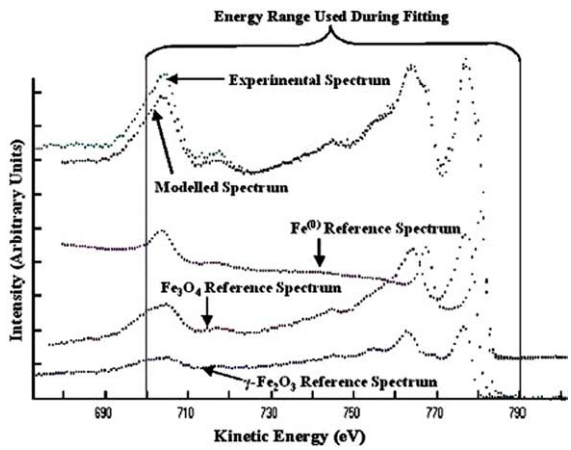

Fig. 5. QUASES^{TM} Generate Fe 2p model of Fe surface exposed to 1.3×10^2 Pa O_2 for 120 s at 27 °C. The spectrum indicated here corresponds to the model shown in Fig. 6(c). Its corresponding QUASES^{TM} Analyze model spectrum is shown in Fig. 3.

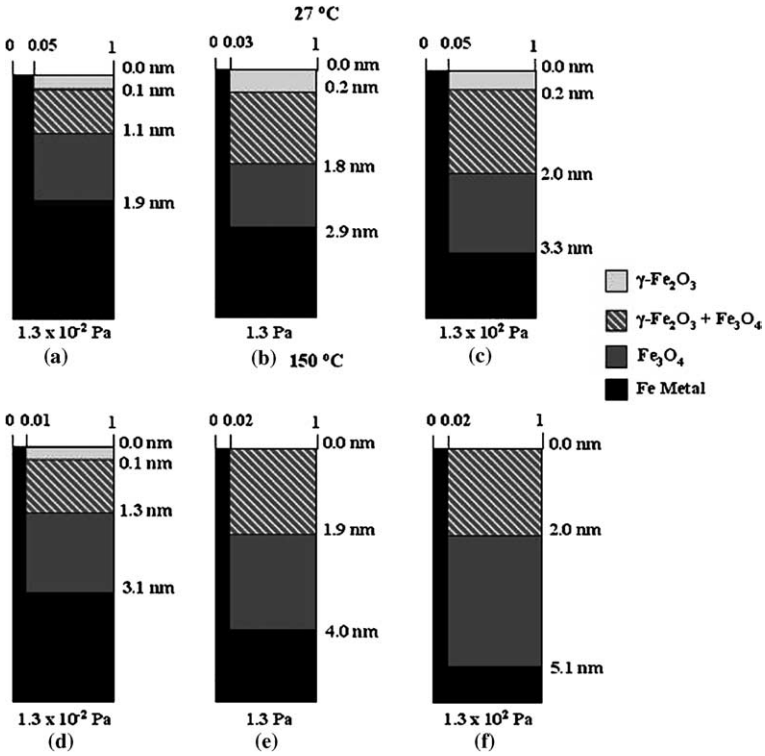

Fig. 6. Profiles of oxide thicknesses and compositions determined using QUASES^{TM} Generate for samples exposed to O_2 for 120 s: (a) 1.3×10^{-2} Pa, 27 ± 2 °C, (b) 1.3 Pa, 27 ± 2 °C, (c) 1.3×10^{2} Pa, 27 ± 2 °C, (d) 1.3×10^{-2} Pa, 150 ± 1 °C, (e) 1.3 Pa, 150 ± 1 °C, (f) 1.3×10^{2} Pa, 150 ± 1 °C.

and γ-Fe_2O_3 was found in all cases examined; this is believed to represent a solid oxide solution where some Fe^{2+} ions of Fe_3O_4 have undergone oxidation. The overall oxide thickness determined by Generate using Fe 2p spectra was found to increase with dose, in good accord with the thicknesses obtained using Analyze and the O 1s spectra. However, the data obtained by Generate provides a much more detailed analysis of the roles of different oxides than has been possible previously. These enhanced analyses provide a new opportunity to develop a more detailed model of the oxidation process. The Generate analysis also shows a small contribution from metallic Fe distributed throughout the oxide structure. This could result from some grain interiors remaining unoxidized.

In Fig. 7, oxide thicknesses determined by QUASES^{TM} Generate are plotted as a logarithmic function of O_2 dose. Fig. 7(a) plots the entire oxide thickness. These results can be directly compared to those obtained using Analyze and the O 1s extrinsic loss data; both are virtually identical for each temperature. The total thickness of Fe_3O_4 formed in the oxide layer consists of the pure Fe_3O_4 layer (shown in dark grey in Fig. 6) along with the Fe_3O_4 layer that underwent additional oxidation to form a layer containing a solid oxide solution. This thickness was found to be little different from the total thicknesses indicated in Fig. 7(a); thus the relationship between oxygen dose and oxide thickness can be analyzed critically with respect to the initial nucleation and growth of Fe_3O_4 on metallic Fe using these results. It appears that a logarithmic relationship between Fe_3O_4 thickness and O_2 dose is maintained over a pressure range of four orders of magnitude, suggesting that changes in O_2 pressure have little effect on the mechanism of growth for this particular oxide phase.

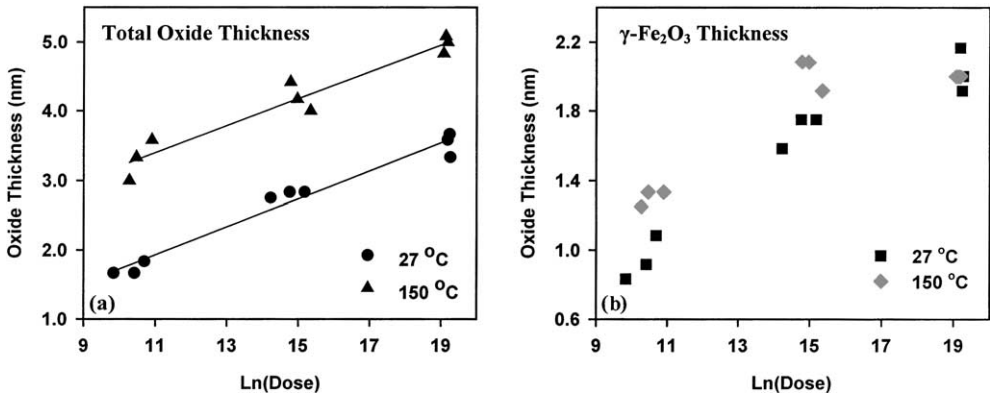

Fig. 7. QUASES™ Generate results showing the total oxide thickness (a) as well as the individual γ-Fe_2O_3 oxide thickness (b).

The growth of the γ-Fe_2O_3 phase was followed using the thickness of the pure γ-Fe_2O_3 along with the thickness of the mixed γ-Fe_2O_3–Fe_3O_4 phase (see Fig. 7(b)). For γ-Fe_2O_3 growth studied over a range of pressures, it was not possible to find a simple logarithmic relationship between dose and the oxide thickness formed. Thus, it appears that the growth of the γ-Fe_2O_3 phase is, in fact, dependent on the concentration of O_2 present.

3.2. Oxidation kinetic studies under different pressure regimes

As a result of the pressure dependent growth observed for the γ-Fe_2O_3 phase on the outer surface, a more detailed investigation of the overall growth kinetics of the oxide film formed on Fe was performed using two specific pressure regimes: 1.3×10^{-2} and 1.3 Pa. In Fig. 8(a), the growth kinetics of the Fe_3O_4 layer are shown (oxide thickness versus log exposure time) for both pressures used. Fig. 8(b) shows the relationships found for the γ-Fe_2O_3 thickness versus log exposure time. Both oxides were found to follow direct logarithmic kinetics rather than inverse logarithmic kinetics. This observation was made based on the overall fit of the respective plots. The inverse logarithmic plots gave an average R^2 value of 0.93, while the direct logarithmic plots gave an average R^2 value of 0.98. For Fe_3O_4, the slopes of the plots

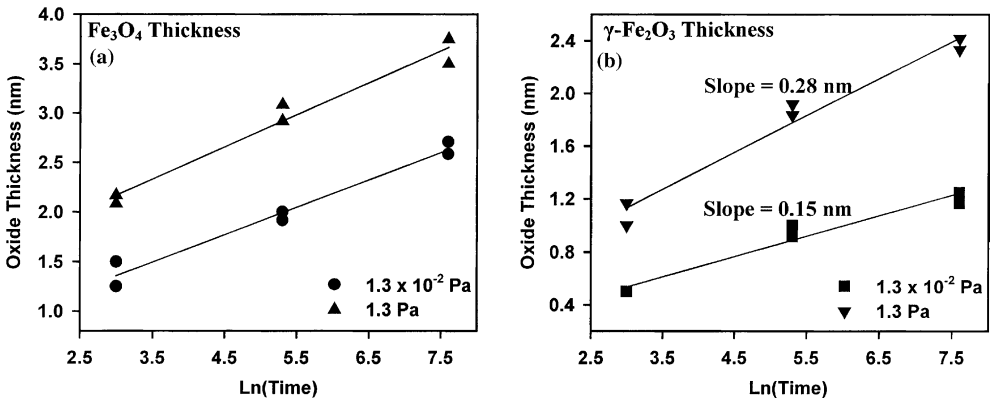

Fig. 8. Kinetic results for Fe_3O_4 (a) and γ-Fe_2O_3 (b) determined using QUASES™ Generate for reaction pressures of 1.3×10^{-2} and 1.3 Pa at room temperature. The results were again found to follow a direct logarithmic relationship with an R^2 value of 0.98 for both the Fe_3O_4 and γ-Fe_2O_3 results whereas the R^2 values for an inverse logarithmic relationship and a parabolic relationship were considerably lower.

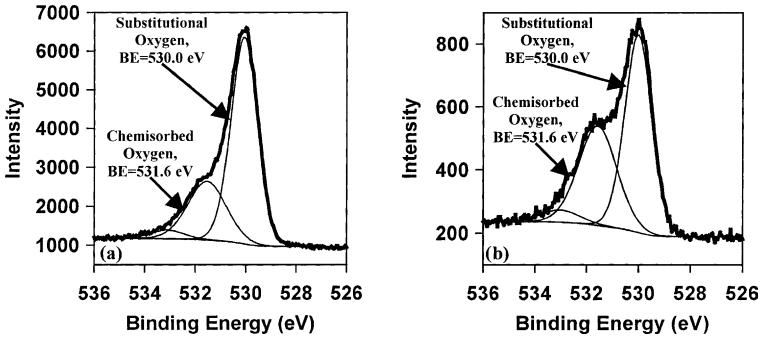

Fig. 9. High resolution XPS O 1s spectra indicating the presence of substitutional and chemisorbed oxygen at electron take-off angles of 90° (a) and 15° (b).

were found to be identical within experimental error. For γ-Fe_2O_3 however, the slope increases substantially as the O_2 pressure increases, thus indicating a significant role for anionic in-diffusion in the formation of the γ-Fe_2O_3 phase.

In addition to changes to the Fe 2p spectra shown in Figs. 1 and 2, changes to the O 1s lineshapes for oxidation at the two pressures investigated were also seen. Fig. 9 represents the O 1s lineshape found for an oxide formed after exposure of Fe to 1.3×10^{-2} Pa of O_2 for 120 s at 27 °C using a 90° (a) and 15° (b) electron take-off angle. The peak at 530.0 eV is assigned to substitutional oxygen in the oxide in accordance with many other studies [4,10,27,30]. The shoulder at 531.6 eV is considered to be from a species associated with the outer surface, as observed by its angular dependence. This species is almost certainly chemisorbed atomic oxygen rather than a hydroxyl adsorbate; since the P_{O_2}/P_{H_2O} ratio in the reaction chamber was $>10^4$.

4. Discussion

Taking the above results into consideration, a detailed mechanism of Fe oxidation can now be presented. Oxygen adsorbs onto the Fe surface with an initial thin oxide layer(s) able to support ion transport being formed due to place-exchange [19,31]. The mechanism of the place-exchange reaction is as follows: oxygen adsorbs onto the metal surface and dissociates to give chemisorbed atomic oxygen, which may interact with the metal atoms located at the surface forming covalent bonds, weakening their attachment to the surrounding metal lattice [19]. The dipole formed between the O and Fe after bonding causes them to exchange places. This form of oxidation is only able to form a few monolayers of oxide before it terminates and a new process must be invoked to continue oxidation [31]. The new process requires an electric field produced by tunnelling electrons from the metal to the adsorbed oxygen to be formed. Outward cation diffusion through vacancies appears to control the growth of Fe_3O_4 because its growth was found to be independent of the O_2 pressure, whereas anion diffusion inwards through interstitial sites and grain boundaries is responsible for the growth of γ-Fe_2O_3. To allow diffusion in either direction, the electric field strength must be sustained and this requires the potential to increase as the oxide thickness increases.

The reaction rates (nm/s) were calculated using the direct logarithmic model [19] (indicated above as Eq. (2)) since it proved to best fit the data; these are shown in Fig. 10. The results indicate that, even for oxides of differing thicknesses, the reaction rates at the two different pressures studied are essentially the same. This observation requires that oxygen adsorption and/or oxidation via place-exchange be rate-limiting, and not cationic or anionic diffusion. Fig. 10 also indicates that the reaction rates decelerate exponentially over time for both pressures studied, indicating that as the

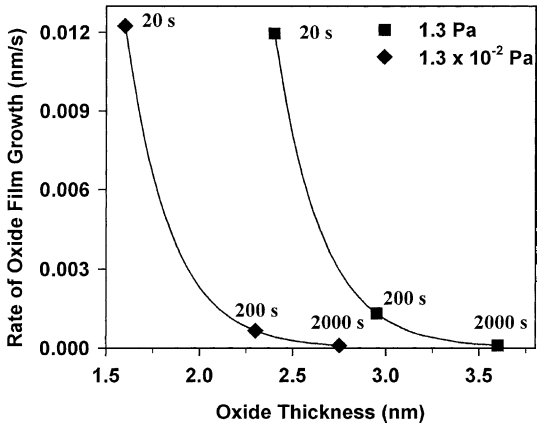

Fig. 10. Plots of the reaction rate versus oxide thicknesses determined using QUASES™.

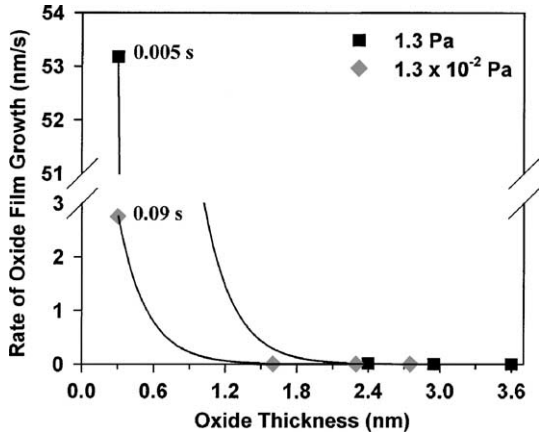

Fig. 11. Calculated and experimentally derived reaction rates indicating the time at which each reaction began. The starting times refer to the point where the oxide had a proposed thickness of 0.3 nm due to the formation of a mono-layer of oxide by place-exchange.

electric field strength breaks down so does the ability of the oxide layer to grow. This has been supported by the suggestion that as an oxide film thickens, its work function increases, which impedes the travel of electrons to the surface thus restricting its overall growth [32]. The closeness of the rates found at the two pressures studied suggests that the sizes of the electric fields formed are proportional to each other and therefore break down within the same time period.

Using the kinetic equations found for the 1.3×10^{-2} and 1.3 Pa reactions, the reaction rates were able to be extrapolated backward to an oxide thickness of 0.3 nm, which is attributed to a single mono-layer of oxide formed via place-exchange. As discussed above, this layer must form before the field driven mechanism can begin. This particular thickness was chosen because it represents the spacing in between Fe atoms of a FeO lattice [3], which has been chosen to represent the place-exchange formed oxide. Both the calculated and experimentally derived rates are shown in Fig. 11. The oxide thickness from the 1.3×10^{-2} Pa reaction was found to begin forming via the field driven mechanism after an exposure of about 0.09 s to O_2, while the 1.3 Pa reaction began after only 0.005 s—a considerable difference. The increased initial rate for the 1.3 Pa reaction results from a larger electric field being able to be formed. The idea of increased field strength with increasing reaction pressure has been suggested previously [33].

The time at which oxidation began was compared to the time required for a single monolayer of oxygen to adsorb to the surface of the Fe at room temperature. Using an approximate atom surface density of 10^{15} atoms/cm^2 [34], the adsorption time for oxygen at 1.3 and 1.3×10^{-2} Pa was found to be 2.0×10^{-4} and 2.0×10^{-2} s, respectively. This result indicates that, for both reactions, oxidation did not begin until well after the adsorption process had completed. The difference in time between the time required for adsorption to occur and the time at which oxidation via the field driven mechanism began can be attributed to the amount of time required for the place-exchange reaction to occur. This observation suggests that it is the initial place-exchange reaction that is rate-limiting. The rate at which the place-exchange reaction occurs must be dependant upon the amount of oxygen present at the time of reaction [19]. At lower reaction oxygen pressures, the oxide would therefore form slower than at higher pressures, which is why the reaction times for place-exchange suggested above differed greatly depending on if the reaction occurred at an oxygen pressure of 1.3×10^{-2} or 1.3 Pa. It should also be noted that the field formed during the 1.3 Pa reac-

tion would be strong since a substantial layer of oxygen would adsorb onto the Fe surface before place-exchange was finished, allowing it to accept many more tunnelling electrons than in the case of the 1.3×10^{-2} Pa reaction. This increased potential would therefore allow for a greater overall oxide thickness to be formed.

After the above discussion, we can now examine the temperature dependence of the oxidation reaction. At temperatures around 150 °C, thermionic emission of electrons through the oxide can occur, which in combination with the flux of tunnelling electrons would allow for a stronger electric field to be formed [34]. The increased field strength would therefore enable formation of a greater oxide thickness. This was seen specifically for the Fe_3O_4 layer, but not for the γ-Fe_2O_3 layer since its growth was controlled by anionic diffusion and depended on the amount of oxygen available.

5. Conclusions

The use of the two QUASES^{TM} programs allowed for the in depth study of not only the overall oxide film but also the growth mechanisms of the two individual oxide species found (Fe_3O_4 and γ-Fe_2O_3). The measurements have lead to a model wherein the contributions of both cationic and anionic diffusion to the growth of the individual oxides is proposed, as opposed to previously proposed mechanisms, which account only for cation diffusion of Fe ions. The reaction kinetics were found to follow the direct logarithmic system with the experimental reaction rates for the two reaction pressures examined being found to be similar. Considerable differences were found for the initial reaction rate after place-exchange had occurred as well as the exposure time after which oxidation began via the field driven mechanism, which was explained by a difference in the magnitude of the electric field formed. After the appropriate electric field was produced, vacancies and ion channels capable of supporting diffusion became available, allowing the growth of the oxide layer to proceed. The overall film thickness produced depended on the strength of the electric field formed. The rate-limiting step of the reaction was determined to be the formation of a thin oxide layer by place-exchange.

Acknowledgments

The authors would like to acknowledge the Natural Sciences and Engineering Research Council of Canada (NSERC) for funding this work.

References

[1] T.E. Graedel, R.P. Frankenthal, J. Electrochem. Soc. 137 (1990) 2385.
[2] F.P. Fehlner, M.J. Graham, in: P. Marcus, J. Oudar (Eds.), Corrosion Mechanisms in Theory and Practice, Marcel Dekker Inc., New York, 1995, p. 123.
[3] R.M. Cornell, U. Schwertmann, The Iron Oxides; Structures, Properties, Reactions, Occurrence and Uses, VCH, New York, 1996.
[4] C.R. Brundle, T.J. Chuang, K. Wandelt, Surf. Sci. 68 (1977) 459.
[5] B. Sinkovic, P.D. Johnson, N.D. Brookes, A. Clarke, Phys. Rev. Lett. 65 (1990) 1647.
[6] T.-C. Lin, G. Seshadri, J.A. Kelber, Appl. Surf. Sci. 119 (1997) 83.
[7] S.J. Roosendaal, B. van Asselen, J.W. Elsenaar, A.M. Vredenberg, F.H.P.M. Habraken, Surf. Sci. 442 (1999) 329.
[8] N. Cabrera, N.F. Mott, Rep. Prog. Phys. 12 (1948–1949) 163.
[9] M.J. Graham, S.I. Ali, M. Cohen, J. Electrochem. Soc. 117 (1970) 513.
[10] A. Srinivasan, K. Jagannathan, M.S. Hegde, C.N.R. Rao, Indian J. Chem. 18A (1979) 463.
[11] A.G. Goursat, W.W. Smeltzer, Oxid. Met. 6 (1973) 101.
[12] T. Do, N.S. McIntyre, Surf. Sci. 440 (1999) 438.
[13] H. Konno, M. Nagayama, in: Proceedings of the 4th International Symposium on the Passivity of Metals, Electrochemical Society, Princeton, 1978, p. 585.
[14] P.C.J. Graat, M.A.J. Somers, ECASIA 95, Wiley, Monteux, 1995, p. 611.
[15] S. Tougaard, Surf. Interf. Anal. 26 (1998) 249.
[16] J.E. Castle, R. Ke, J.F. Watts, Corros. Sci. 30 (1990) 771.
[17] S. Tougaard, QUASES^{TM}, Version 4.4, Software for Quantitative XPS/AES of Surface Nano-Structures by Analysis of the Peak Shape and Background, 2000.
[18] A.P. Grosvenor, B.A. Kobe, N.S. McIntyre, S. Tougaard, W.N. Lennard, Surf. Interf. Anal. 36 (2004) 632.
[19] D.D. Eley, P.R. Wilkinson, Proc. R. Soc. London A 254 (1960) 327.
[20] P.A. Lee, K.F. Stork, B.L. Maschhoff, K.W. Nebesny, N.R. Armstrong, Surf. Interf. Anal. 17 (1991) 48.
[21] N. Fairley, CasaXPS Version 2.2.19, 1999–2003.

[22] R.P. Gupta, S.K. Sen, Phys. Rev. B 10 (1974) 71.
[23] R.P. Gupta, S.K. Sen, Phys. Rev. B 12 (1975) 15.
[24] N.S. McIntyre, D.G. Zetaruk, Anal. Chem. 49 (1977) 1521.
[25] M.C. Biesinger, C. Brown, J.R. Mycroft, R.D. Davidson, N.S. McIntyre, Surf. Interf. Anal., in press.
[26] S. Doniach, M. Sunjic, J. Phys. C 3 (1970) 285.
[27] M.W. Roberts, P.R. Wood, J. Electron Spectrosc. Relat. Phenom. 11 (1977) 431.
[28] S. Tanuma, C.J. Powell, D.R. Penn, Surf. Interf. Anal. 11 (1988) 577.
[29] S. Tougaard, Surf. Interf. Anal. 11 (1988) 453.
[30] M.W. Roberts, Appl. Surf. Sci. 52 (1991) 133.
[31] F.P. Fehlner, N.F. Mott, in: Oxidation of Metals and Alloys; Papers Presented at a Seminar of the American Society for Metals, October 17 and 18, 1970, American Society for Metals, Metals Park, 1971, p. 37.
[32] D. Vlachos, N. Panagiotides, S.D. Foulias, J. Phys.: Condens. Matter 15 (2003) 8195.
[33] B.L. Maschhoff, N.R. Armstrong, Langmuir 7 (1991) 693.
[34] G.W.R. Leibbrandt, G. Hoogers, F.H.P.M. Habraken, Phys. Rev. Lett. 68 (1992) 1947.